Optimizing the Fabrication of Polyimide Shells

Introduction

Polyimide is being developed as an ablator material for inertial confinement fusion (ICF) targets because of its superior mechanical and thermal properties.[1] A typical target design for the OMEGA laser system consists of a spherical shell, 1 mm in diameter and 1 μm in wall thickness, with a 100-μm-thick layer of solid deuterium and tritium (DT) uniformly deposited on the inner surface. To achieve this, the shells must be both strong and permeable so that they can be filled quickly with DT gas and survive the pressure gradient created in subsequent treatments, including cooling to below 18.9 K and layering by differential heating. Material properties that determine the performance of shells as targets include gas permeability, Young's modulus, tensile strength, and elongation at break.[2]

Fabrication of spherical polyimide shells has been demonstrated using a vapor deposition polymerization (VDP) method, and preliminary characterization of the shell properties has been conducted.[2–4] In this work, a parametric study was performed on the fabrication process of polyimide shells. The production rate, yield, and reproducibility of the process were optimized. The shells were thoroughly characterized to determine the material properties, microstructures, and surface finish, which were then correlated with the processing parameters. The permeability was also determined at cryogenic temperatures between 130 K and 295 K.

Experimental

1. Fabrication

a. Materials. 1,2,4,5-benzenetetracarboxylic dianhydride (PMDA) (97% purity) and 4,4′-oxydianiline (ODA) (99+% purity; zone refined) were purchased from Aldrich Chemical and used as received. Spherical shells, ~910 μm in diameter with a 7- to 17-μm wall thickness and >99.8% sphericity, made of thermally depolymerizable poly-α-methylstyrene (PAMS) with a molecular weight (MW) of 400,000 were received from General Atomics and used as mandrels without further treatment.

b. Deposition. The fabrication process involved two steps. PMDA and ODA were vapor deposited to form poly(amic acid) (PAA) on either PAMS mandrels or flat substrates. The PAA layer was then converted into polyimide by thermal imidization. In this process, the PAMS mandrels depolymerized and permeated out of the nascent polyimide layer, resulting in freestanding shells. The chemical reaction scheme is shown in Fig. 88.28.

A schematic of the deposition system is shown in Fig. 88.29. The two monomers were separately sublimed from two evaporators directed toward a rotating coating stage.[3] The vacuum chamber was maintained at 4.8 to 5.2×10^{-6} Torr throughout deposition. The individual deposition rates of PMDA and ODA
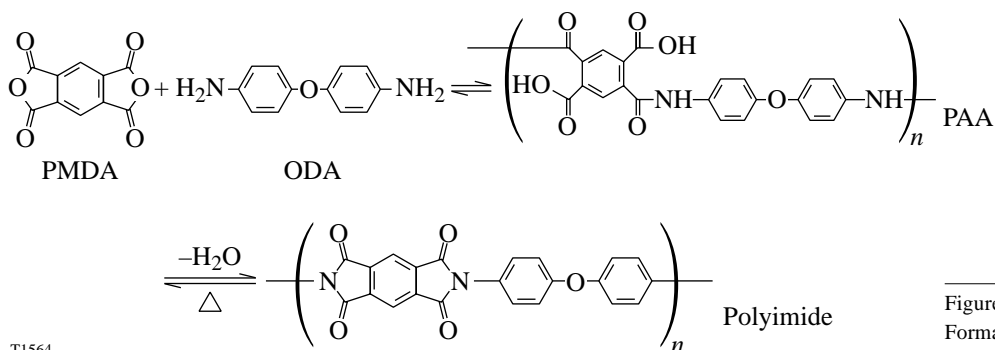
Figure 88.28
Formation of polyimide from PMDA and ODA.

T1564

were measured by depositing each of them separately onto 0.3-cm² PAMS films, which were weighed, before and after deposition, to an accuracy of ±0.05 μg using a microbalance (Cahn model 4700). The monomer deposition rates were measured for discrete evaporator temperatures and substrate positions to determine the conditions that yielded equimolar deposition of the monomers. A 3 × 5-cm² shutter plate was used to shield the substrate for approximately 30 min until the steady-state deposition rates were reached.
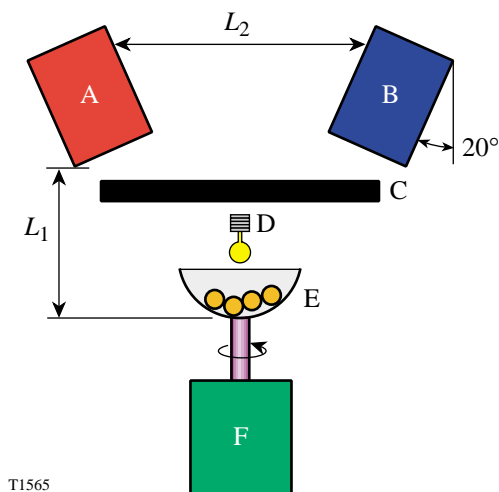

Figure 88.29
Schematic of the deposition system inside the vacuum chamber. A: evaporator for ODA; B: evaporator for PMDA; C: shutter; D: tungsten lamp filament; E: rotating pan with shells; F: motor. Dimensions: L_1 = 3 cm; L_2 = 5 cm.

Batches of 20 to 60 PAMS mandrels were over-coated in a 1-cm-diam hemispherical aluminum holder rotating at 60 to 120 rpm.[5] The static charge created by the motion of the mandrels was neutralized by flooding the entire holder with electrons from a biased tungsten filament (12 V; 20 mA) 0.5 cm above the holder. To examine the effect of a heated substrate, the temperature of the PAMS mandrels was raised from room temperature to 140°C. This was achieved by clamping the shaft of the rotating pan between two copper fingers that were connected to a cartridge heater. The temperature was controlled with an OMEGA CN9001 temperature controller. The pan was preheated at 140°C for 2 to 3 h before deposition began.

Flat films were deposited on either silicon wafers (1 × 1 cm²) or sodium chloride disks (1.3-cm diameter and 0.1-cm thickness; purchased from International Crystal Labora-

tory), which were also rotated at 60 to 120 rpm. The deposition rate was ~7 μm/h for flat films and ~3 μm/h for shells at room temperature.

c. Imidization. The as-deposited PAA shells were imidized in a NEY Centurion VPM vacuum furnace with programmable temperature (accuracy = ±0.1°C). The furnace was purged by a constant 7.5-cm³/min flow of nitrogen or air throughout the imidization process. The temperature cycle consisted of a ramp-up (0.1, 0.5, or 1°C/min) from 25 to 300°C, a soak at 300°C for a predetermined duration (1, 3, or 6 h), and cooldown to 25°C at 5°C/min. Images of the shells during imidization were recorded and analyzed to monitor the changes in shell diameter with temperature. Imidized flat films were detached from the substrates by soaking in de-ionized water at 90°C for 24 to 48 h. The films were then dried at 80°C under vacuum for 24 h.

2. Characterization
a. Chemical analysis. Fourier transform infrared (FTIR) spectra were obtained using films approximately 1 μm thick deposited on sodium chloride disks. The elemental composition was determined by combustion analysis performed by Oneida Research Services using freestanding films with mass of approximately 10 mg. Solubility was examined by soaking films and shells in concentrated sulfuric acid (97%) at room temperature. The size of the samples was monitored using an optical microscope throughout soaking.

b. X-ray diffraction (XRD). The tested samples included (1) freestanding films (1 cm × 1 cm × 25 μm), (2) shells, and (3) flat films made of 10 to 20 flattened shells. A Rigaku D2000 Bragg-Brentano diffractometer[6] equipped with a copper rotating anode, diffracted beam graphite monochromator, and scintillation detector was used to obtain reflection-mode diffraction patterns from film samples. Data were collected as continuous scans, at a scan rate of 2° 2θ/min. A Bruker AXS microdiffractometer[7] equipped with a copper rotating anode, Goebel mirrors, a 0.5-mm collimator, and a two-dimensional general area detector diffraction system (GADDS) was used to obtain transmission-mode diffraction patterns for shell and film samples and reflection-mode diffraction patterns for shell samples. Each data set was collected until 10⁷-count total integrated intensity was achieved.

c. Dimensions and surface finish. Shell diameter was measured to an accuracy of ±1 μm using a Nikon Optiphot microscope, and the wall thickness was calculated from mass and density. The shell mass was measured to an accuracy of

±0.05 μg using a microbalance, and the density was measured to an accuracy of ±0.001 g/cm^3 using a density column (performed by General Atomics). The wall thickness obtained by this method was confirmed by SEM (scanning electron microscope) micrographs of the wall cross sections obtained on a LEO 982 Field Emission SEM. The thickness of flat films was measured using a Rank Taylor Hobson Talysurf profilometer to an accuracy of 0.1 μm.

The shell's surface finish was characterized by sphere-mapping (performed by General Atomics) and by using a SEM. Sphere maps were measured for thin-walled (1.5- to 1.8-μm) shells that were slightly inflated (~1%) by 4- to 6.5-atm internal pressure of nitrogen. The permeability of nitrogen through the shell wall was sufficiently low to maintain the inflation for ~24 h. The same shells were measured again when deflated to compare the surface finish with or without inflation.

d. Property measurements. One hundred to two hundred shells prepared under each imidization condition were measured for gas permeability and mechanical properties. The permeability was determined by measuring the time constant. Young's modulus, tensile strength, and elongation at break were determined by a burst/buckle test. Detailed descriptions of the test procedures can be found elsewhere.[3,8] Helium permeability at cryogenic temperatures (156 K to 298 K) was determined for Kapton HN and vapor-deposited flat films (dimension = 1 cm × 1 cm × 25 μm) using a setup reported elsewhere,[3] with the addition of a helium leak detector (Edwards Spectron 600D) to measure the helium permeation rates through the films.[9]

Results and Discussion

1. Yield and Reproducibility of the Fabrication Process
a. Deposition. Maintaining the stoichiometric ratio (1:1) of monomers when depositing PAA is critical since non-stoichiometric deposition results in greatly deteriorated properties and surface finish.[10–13] The monomers must also be uniformly deposited over the entire substrate surface. The spatial variation of the monomer deposition rates on the substrate plane is shown in Fig. 88.30 (note that the X-Z plane is the plane of symmetry for the two evaporators). The dependency of the monomer deposition rates on the evaporator temperature is shown in Fig. 88.31. The evaporator temperatures that yielded equimolar monomer deposition were PMDA = 153°C and ODA = 126°C. The substrate located at the center of the chamber floor [(0,0,0) in Fig. 88.30] was minimized in size (1 × 1 cm^2 for flat films; ~0.5 × 0.5 cm^2 for shells) and rotated at 120 rpm to reduce the spatial variability. Figure 88.32

illustrates the smooth surface of a typical shell deposited under the above conditions.

b. Imidization. The key factor that determines the yield of polyimide shells is the stress generated during imidization, which can rupture the shells if not carefully controlled. The main source of stress is the depolymerization of the PAMS mandrels into gaseous products at elevated temperatures. Depending on the depolymerization rate, the products may be unable to permeate out of the polyimide layer at the rate they are produced, creating a pressure differential that inflates the shells.

The changes in shell diameter during imidization under various heating rates and atmospheres are shown in Fig. 88.33. The shells imidized in air inflated more abruptly and at a lower
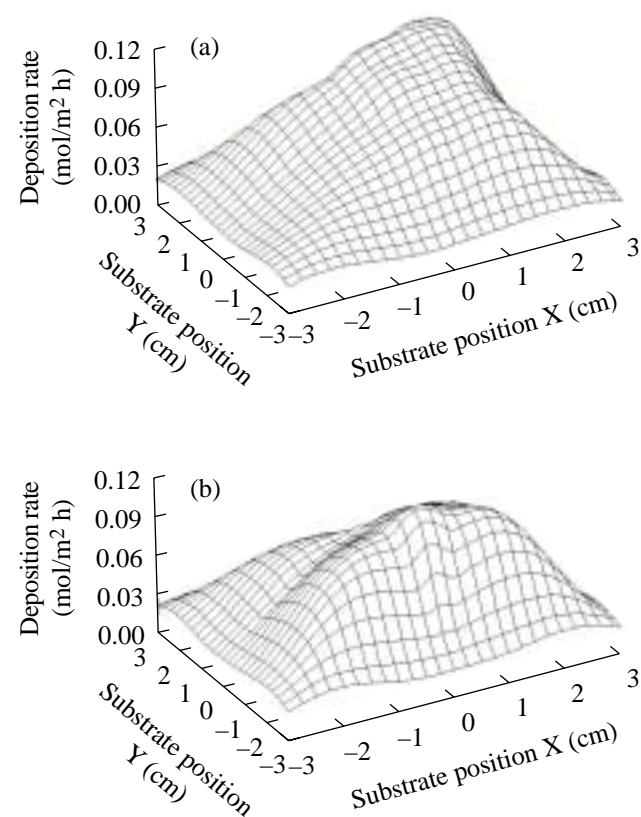

T1570

Figure 88.30
Spatial variation of the monomer deposition rates on the substrate plane: (a) PMDA (153°C), (b) ODA (126°C). Note that the X-Z plane is the plane of symmetry for the two evaporators. The separation between the evaporators is 5 cm, and the vertical distance between the substrate and evaporator planes is 3 cm, as shown in Fig. 88.29.

temperature than those imidized in nitrogen. This was attributed to the lower initiation temperature and higher reaction rate of the depolymerization of PAMS in the presence of oxygen. The yield of air-imidized shells was reduced as a result of this drastic inflation, as summarized in Table 88.II. In a nitrogen atmosphere, shells inflated more at higher heating rates due to the more rapid depolymerization of PAMS (Fig. 88.33), and the yield was lowered (Table 88.II). Imidizing at 0.1°C/min in a nitrogen atmosphere minimized the inflation and thus provided the highest yield.

The chemical composition of the polyimide shells and films produced by the optimized process agreed with that of the commercial PMDA-ODA films (Kapton®), as shown in the FTIR spectra (Fig. 88.34) and the combustion analysis data (Table 88.III).
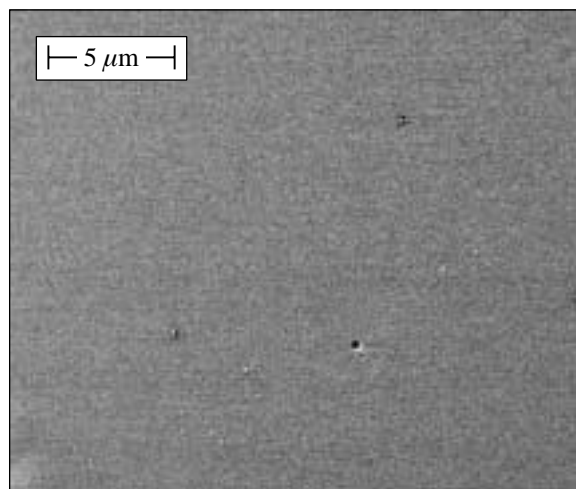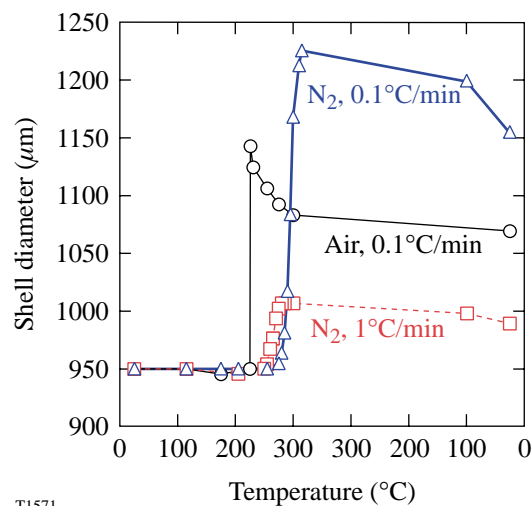

T1569

Figure 88.32
SEM micrograph of the outer surface of a 4-μm-thick polyimide shell.
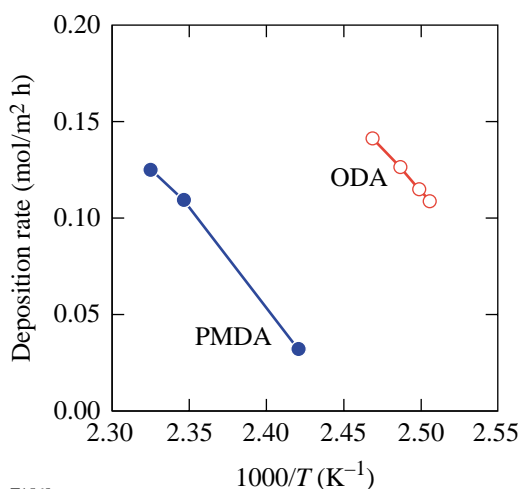
T1568

Figure 88.31
Dependency of the monomer deposition rates on the evaporator temperature. The deposition rates were measured with 0.3×0.3-cm^2 PAMS films located at (0,0,0) of Fig. 88.30.

T1571

Figure 88.33
Changing shell diameter with imidization temperature for three imidization conditions: (a) N$_2$, 0.1°C/min, (b) air, 0.1°C/min, and (c) N$_2$, 1°C/min. The shells remained spherical throughout imidization.

Table 88.II: Yield of polyimide shells under different imidization conditions.

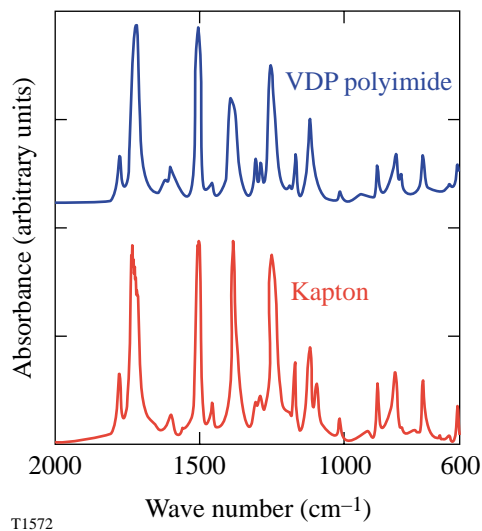|	Air 0.1°C/min	N$_2$ 0.1°C/min	N$_2$ 0.5°C/min	N$_2$ 1.0°C/min
Yield (%)	60	100	90	60

Figure 88.34
FTIR spectra of vapor-deposited polyimide (VDP) and Kapton®. The VDP sample was imidized at 0.1°C/min in N_2 for 6 h. The Kapton spectrum was obtained using a 8-μm-thick Kapton® HN film (DuPont).

Table 88.III: Atomic composition of VDP polyimide (imidized at 0.1°C/min in N_2; 6 h at 300°C) by combustion analysis. The formula of polyimide is $C_{22}H_{10}N_2O_5$.

	Atomic percent (%)			
	C	H	N	O
VDP (±0.2)	55.3	26.8	5.3	12.7
By formula	56.4	25.7	5.1	12.8

2. Properties of Polyimide Shells

The measured properties of polyimide shells agree with the literature values of commercial Kapton® films,[14] as shown in Table 88.IV. The experimental test matrix employed to obtain these properties used five to ten shells per batch; ten to twenty batches were tested to obtain batch-to-batch reproducibility. The narrow uncertainty intervals listed in Table 88.IV confirm the reproducibility of the process.

3. Effects of Imidization Conditions

Different imidization conditions resulted in different permeability, tensile strength, and flexibility (ultimate strain) but had little effect on the Young's modulus of the shells. The results can be summarized as follows:

a. Imidizing atmosphere (N_2 versus air). The properties of N_2- and air-imidized polyimides are compared in Table 88.V. Imidizing in air instead of nitrogen increased the permeability by ~100% while reducing the strength by ~25%. The elongation at break was also decreased by ~50%. The air-imidized shells possessed lower crystallinity than N_2-imidized shells, as indicated by the x-ray diffraction patterns in Fig. 88.35, where the peak associated with the 002 lattice planes is substantially weaker in the air-imidized samples.

The FTIR spectra in Fig. 88.36 show that the air-imidized samples retained a weak anhydride peak at 1850 cm^{-1}, indicating that a small fraction of the imide groups had been hydrolyzed into anhydride. This may result in a shortened polymer chain length that generally reduces the tensile strength and elongation at break of polymeric materials.[15] Both air- and N_2-imidized shells were cross-linked, as indicated by the fact that they were insoluble in concentrated sulfuric acid.[16] The distinct properties of the air-imidized samples may be attributed to their lower crystallinity and MW.

Table 88.IV: Properties of polyimide shells (imidized at 0.1°C/min in N_2; 6 h at 300°C) and the literature values for Kapton®. E = Young's modulus, σ = tensile strength, and ε = elongation at break.

	Mechanical Properties			Gas Permeability (mol·m/m²·Pa·s)			
	E (GPa)	σ (MPa)	ε	He × 10¹⁶	H_2 × 10¹⁶	D_2 × 10¹⁶	N_2 × 10¹⁸
VDP shells	3.2±0.1	280±19	0.27±0.02	4.9±0.1	3.6±0.1	3.5±0.1	3.9±0.2
Kapton®[13]	2.5	231		8.2	4.9	4.4±0.1*	12
*Measured experimentally with 25-μm-thick Kapton® HN films (DuPont). (Literature value of D_2 permeability through Kapton is unavailable.)							

b. _Imidizing rate._ The properties of polyimide imidized at different heating rates are shown in Table 88.VI. Helium permeability increased with the heating rate, while the tensile strength and flexibility showed an opposite trend. The samples imidized at 1°C/min became soluble, suggesting that the fast heating rate had eliminated cross-linking. The higher permeability and lower tensile properties of the shells imidized at 1°C/min may be attributed to the absence of cross-linking.[17–19]

The XRD patterns of shells imidized at 1°C/min and 0.1°C/min are compared in Fig. 88.37. The relative intensity of the 002 peak showed that the crytallinity was lower in the 1°C/min sample than in the 0.1°C/min sample. This provides another explanation for the differences in the properties. The
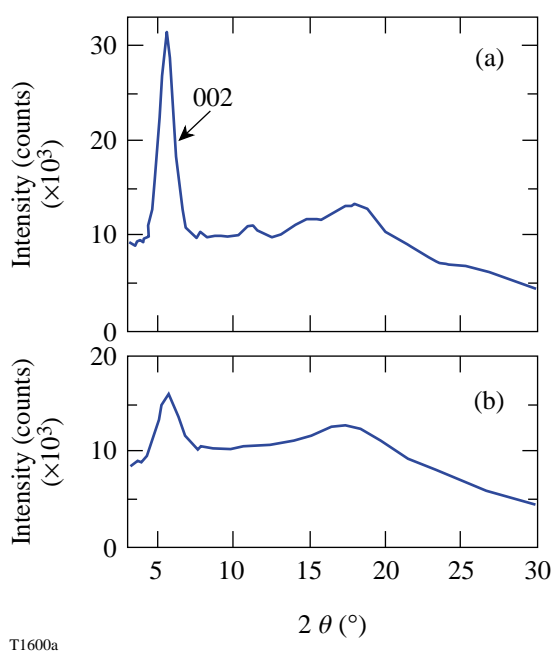
greater strain/stress experienced by the shells imidized at 1°C/min, as shown in Fig. 88.33, is believed to hinder the polyimide molecules from crystallizing.

c. _Imidization time at 300°C._ As shown in Table 88.VII, the helium permeability, tensile strength, and flexibility increased with the duration for which the samples were cured at 300°C. The samples imidized for 1 h dissolved completely in sulfuric acid, while the samples imidized for more than 3 h were insoluble. As displayed in the FTIR spectra (Fig. 88.38), the intensity of the imide peaks ($\sim$1780 and 1380 cm^{-1}) increased with the cure time (no further effect was observed after 6 h at 300°C). The FTIR spectra and solubility results indicate that imidization was incomplete and that cross-linking reactions had not taken place until after 3 h of curing. The low tensile properties and high solubility of the 1-h-cured shells were attributed to the absence of cross-linking and/or lower MW due to incomplete imidization.
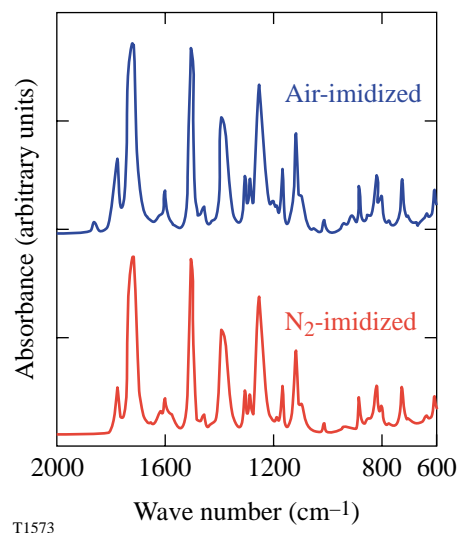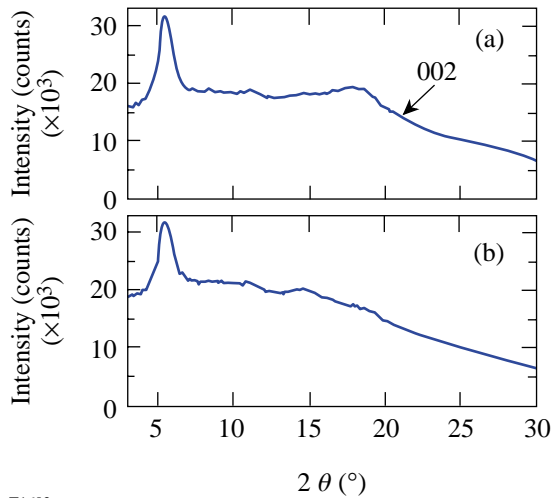

Figure 88.35
1-D x-ray microdiffractometer patterns integrated from 2-D transmission patterns of (a) N$_2$-imidized and (b) air-imidized samples.

Figure 88.36
FTIR spectra of air- and N$_2$-imidized VDP polyimide.

Table 88.V: Properties of N$_2$- and air-imidized VDP polyimide. The permeability and solubility were measured with both film and shell samples, and the other properties were measured with shells only. The imidization conditions (0.1°C/min; 6 h) were the same except for the atmosphere.
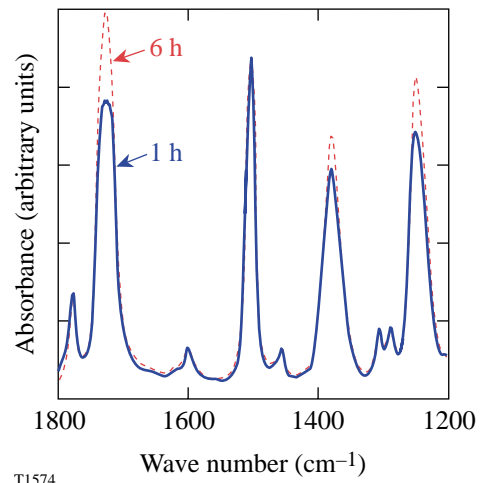
Imidizing conditions	Mechanical Properties			Gas Permeability (mol·m/m^2·Pa·s)			Solubility in H$_2$SO$_4$
	E (GPa)	σ (MPa)	ε	He $\times 10^{16}$	D$_2$ $\times 10^{16}$	N$_2$ $\times 10^{18}$	
N$_2$	3.2±0.1	280±19	0.27±0.02	4.9±0.1	3.5±0.1	3.9±0.2	insoluble
Air	3.0±0.2	191±11	0.13±0.03	11.7±0.6	7.6±0.5	8.5±0.2	insoluble

Figure 88.37
1-D x-ray microdiffractometer patterns integrated from 2-D transmission patterns of shells imidized at (a) 0.1°C/min and (b) 1°C/min.

Figure 88.38
FTIR spectra of VDP polyimide imidized for 1 h and 6 h at 300°C.

Table 88.VI: Properties of VDP polyimide imidized at different heating rates. The solubility was tested with both film and shell samples, and the other properties were measured with shells only. The imidization conditions (nitrogen; 6 h) were the same except for the heating rate.

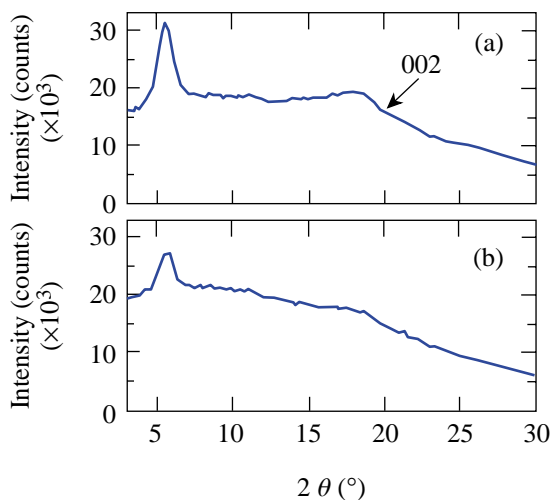| Imidizing conditions	Mechanical Properties			He Permeability $\times 10^{16}$ (mol·m/m^2·Pa·s)	Solubility in H_2SO_4
	E (GPa)	σ (MPa)	ε		
0.1°C/min	3.2±0.1	280±19	0.27±0.02	4.9±0.1	insoluble
0.5°C/min	3.3±0.3	230±26	0.08±0.02	5.3±0.1	insoluble
1.0°C/min	3.3±0.3	136±6	0.03±0.01	5.6±0.2	soluble

Table 88.VII: Properties of VDP polyimide shells imidized for different durations at 300°C. The solubility was tested with both film and shell samples, and the other properties were measured with shells only. The imidization conditions (nitrogen; 0.1°C/min) were the same except for the duration.

Imidizing conditions	Mechanical Properties			He Permeability $\times 10^{16}$ (mol·m/m^2·Pa·s)	Solubility in H_2SO_4
	E (GPa)	σ (MPa)	ε		
1 h	3.4±0.2	100±10	0.15±0.03	4.1±0.1	soluble
3 h	3.2±0.1			4.6±0.1	insoluble
6 h	3.2±0.1	280±19	0.27±0.02	4.9±0.1	insoluble

4. Biaxial Straining and Permeability

Approximately 150 imidized shells that had been inflated with a biaxial strain of ~0.25 were tested for permeability. The results are summarized in Table 88.VIII. The permeability of the shells increased; however, the magnitude of the increase fell into two categories: ~1/3 of the tested shells became ~1000-fold more permeable, while ~2/3 showed a moderate increase of ~25%. Upon heating to 350°C (within the reported T_g range for polyimide)[14] in nitrogen for 1 h, these shells were recovered to their original dimensions and permeability.

The XRD patterns of the shells before and after straining are shown in Fig. 88.39. Straining the shells decreased their crystallinity as indicated by the reduced intensity of the 002 peak. The lowered crystallinity may account for the moderate permeability increase of the strained shells. It is speculated that the ~1000-fold increase in permeability resulted from crazing/
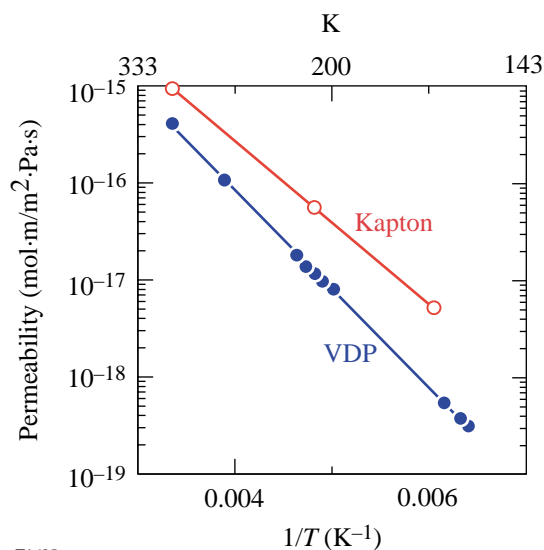
shear-banding, which can create microvoids in the shells and thus greatly expedite permeation.[20] Importantly, the structural integrity of the inflated shells was not affected since they could be repeatedly flattened and recovered by pressure differential and could contain liquid D_2 at cryogenic temperatures.

5. Cryogenic Permeability

The temperature dependency of the helium permeability through Kapton and VDP films is plotted in Fig. 88.40. The data measured with Kapton agree with those reported by S. A. Letts *et al.*[9] Both materials followed the Arrhenius relationship over the measured temperature range. The activation energy for permeation calculated from the data was 19.5 and 16.0 KJ/mol for VDP and Kapton, respectively. The good temperature–permeability correlation will allow the permeability to be estimated in an extended temperature range. The higher activation energy of VDP polyimide may be due to its

T1604a

Figure 88.39
1-D x-ray microdiffractometer patterns integrated from 2-D transmission patterns of (a) pristine and (b) inflated shells.

T1605a

Figure 88.40
Temperature dependency of the helium permeability of VDP and solution-cast polyimide (Kapton) at cryogenic temperatures.

Table 88.VIII: Permeability of polyimide shells before and after straining.

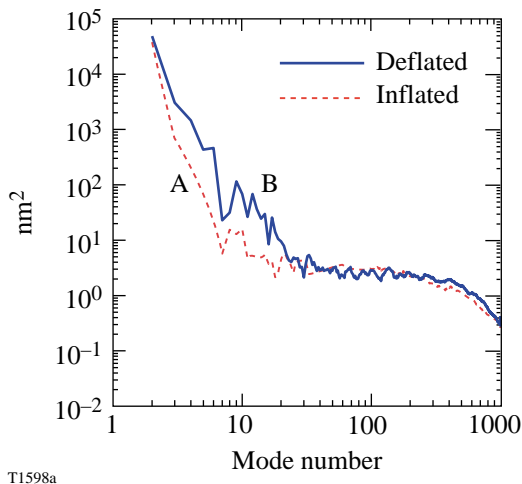|	Permeability (mol·m/m²·Pa·s)		
	Before straining (120 shells)	Biaxially strained (~0.25)	
		80 shells	40 shells
He × 10¹⁶	4.9±0.1	6.2±0.2	NA*
N₂ × 10¹⁸	3.9±0.2	Not measured	500 → 4000

*Permeability too high to measure using current apparatus.

being cross-linked. For polymeric materials, the activation energy is determined by the segmental mobility of the molecules; the segmental mobility is limited when the molecules are cross-linked, resulting in high activation energy.[21]

6. Surface Finish

Figure 88.41 displays the power spectra calculated from the sphere maps of a 1.7-μm-wall shell, inflated and deflated, as described in the **Experimental Section** above. The mode-2 to -20 roughness was reduced when the shell was inflated, suggesting that the low-mode roughness may instead be a "waviness" in the shell wall, which can be eliminated by inflation. Based on this observation, the low-mode roughness of thin-wall cryogenic targets may be significantly reduced since they are kept inflated during application.[22]

The SEM micrographs of the surface of as-deposited shells prepared with unheated and heated substrates are shown in Fig. 88.42. Contrary to our expectation that a heated substrate would re-evaporate unreacted monomers and thus eliminate high-mode roughness (coating-induced bumps),[4] the number density of coating-induced bumps increased with the coating temperature. This may be due to two mechanisms: (1) At higher temperatures the coating rate was slower (50% slower at 140°C than at 25°C), thus the shells experienced more abrasion and collisions, reported to increase surface roughness,[4] over the longer period required to achieve equivalent thickness. (2) The stoichtometry was offset by disproportional re-evaporation of PMDA and ODA, which have different vapor pressures at 120°C to 140°C.
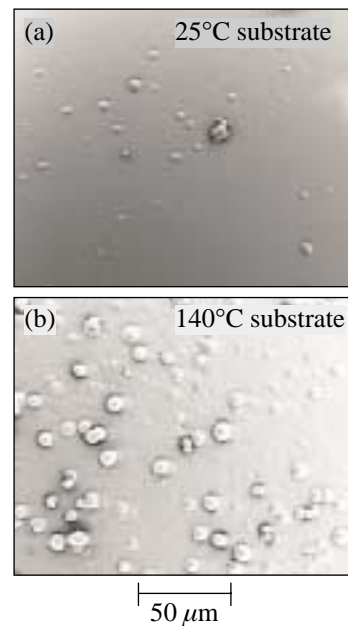
7. Summary

Vapor-deposited polyimide shells had properties equivalent to commercial polyimide films. The fabrication process was studied parametrically to optimize the shell properties, qualities, and yield, and the results can be summarized in the following:

- Strength and surface smoothness of PAA coating were achieved by maintaining an equimolar deposition of the precursor monomers over the substrate surface. Factors that affected the monomer deposition rates included the evaporating temperature and the geometrical arrangement of the substrate.

- The stress generated during imidization due to depolymerization of PAMS mandrels determined the yield of polyimide shells, which could be controlled by varying the imidization conditions. Imidizing at 0.1°C/min in nitrogen atmosphere minimized the stress and provided the highest yield.

- Shells imidized in air were twice as permeable, ~75% as strong, and ~50% as flexible as their counterparts imidized in nitrogen; the Young's modulus was unaffected; and the crystallinity and MW were lower.

T1598a

Figure 88.41
Power spectra of a thin-walled (1.8-μm) polyimide shell: A–inflated (~1%) by 6.5 atm N$_2$; B–deflated after the fill gas permeated out.

T1598b

Figure 88.42
SEM micrographs of the surface of as-deposited shells (6-μm coating) prepared at (a) 25°C and (b) 140°C substrate temperatures.

- Increasing the imidization rate increased the permeability (~25%) and solubility and decreased the strength (~50%) and flexibility (~200%), while maintaining the Young's modulus. The samples imidized at the fastest heating rate became soluble with lower crystallinity.

- Imidizing for less than 3 h at 300°C resulted in lower strength, flexibility, and permeability and produced polyimide that was soluble. The imidization was incomplete at 1 h, which may have led to lower MW and the absence of cross-linking.

- Biaxial straining increased the permeability by up to three orders of magnitude but reduced the crystallinity.

- Inflating thin-wall shells reduced the low-mode surface roughness; heating the substrate during coating increased the high-mode roughness.

Conclusion

Polyimide shells can be reproducibly prepared with dimensions required for ICF targets. The properties and quality of shells can be modified and improved via processing parameters. The modifications in the shell properties are attributed to changes in crystallinity, degree of cross-linking, or molecular weight.

REFERENCES

1. J. J. Sanchez and S. A. Letts, Fusion Technol. **31**, 491 (1997).

2. F. Y. Tsai, E. L. Alfonso, S.-H. Chen, and D. R. Harding, Fusion Technol. **38**, 83 (2000).

3. E. L. Alfonso, S. H. Chen, R. Q. Gram, and D. R. Harding, J. Mater. Res. **13**, 2988 (1998).

4. C. C. Roberts et al., Fusion Technol. **35**, 138 (1999).

5. A. Nikroo and D. Woodhouse, Fusion Technol. **35**, 202 (1999).

6. R. Jenkins and R. L. Snyder, Introduction to X-Ray Powder Diffractometry (Wiley, New York, 1996), Chap. 7, pp. 173–203.

7. B. A. Squires and K. L. Smith, in Advances in X-Ray Analysis, edited by P. K. Predecki et al. (Plenum Press, New York, 1995), Vol. 38, pp. 511–516.

8. F. Y. Tsai, E. L. Alfonso, S. H. Chen, and D. R. Harding, "Processing Vapor-Deposited Polyimide," to be published in the Journal of Physics D.

9. S. Letts et al., presented at the Twelfth Target Fabrication Specialists' Meeting, Jackson Hole, WY, 19–23 April 1998.

10. T. Strunskus and M. Grunze, in Polyimides: Fundamentals and Applications, edited by M. K. Ghosh and K. L. Mittal, Plastics Engineering, Vol. 36 (Marcel Dekker, New York, 1996), pp. 187–205.

11. E. L. Alfonso, F.-Y. Tsai, S.-H. Chen, R. Q. Gram, and D. R. Harding, Fusion Technol. **35**, 131 (1999).

12. R. G. Pethe et al., J. Mater. Res. **8**, 3218 (1993).

13. C. C. Roberts et al., Fusion Technol. **38**, 94 (2000).

14. Kapton® product literature, DuPont™ High Performance Polymers, Circleville, OH 43113.

15. W. Volksen, P. Cotts, and D. Y. Yoon, J. Polym. Sci. B, Polym. Phys. **25**, 2487 (1987).

16. P. M. Cotts and W. Volksen, ACS Symp. Ser. **242**, 227 (1984).

17. C. E. Rogers, in Polymer Permeability, edited by J. Comyn (Elsevier, London, 1985), Chap. 2, pp. 11–73.

18. G. A. Patfoort, Polymers: An Introduction to Their Physical, Mechanical and Rheological Behaviour (Story-Scientia, Gent, Belgium, 1974), pp. 321–323.

19. F. W. Billmeyer, Jr., Textbook of Polymer Science, 3rd ed. (Wiley, New York, 1984), Chap. 12, pp. 330–357.

20. E. H. Andrews, in The Physics of Glassy Polymers, edited by R. N. Haward (Wiley, New York, 1973), pp. 394–453.

21. A. Singh-Ghosal and W. J. Koros, Ind. Eng. Chem. Res. **38**, 3647 (1999).

22. I. Anteby, Ben-Gurion University of the Negev, private communication (1996).